Available online at www.sciencedirect.com
SCIENCE DIRECT®
Pergamon
Cement and Concrete Research 34 (2004) 977–989
CEMENT AND CONCRETE RESEARCH

A study on characteristics of interfacial transition zone in concrete

Kuo-Yu Liao[a,b,*], Ping-Kun Chang[b], Yaw-Nan Peng[a], Chih-Chang Yang[c]

[a]Department of Civil Engineering, National Chiao Tung University, 10F-2, Number 10, Lane 157, Cihhuei, 3rd Street, 1001 Ta Hsueh Road, Hsinchu 300, Taoyuan County, Taiwan 320, Taiwan, ROC
[b]Department of Civil Engineering, Van Nung Institute of Technology, 1, Van Nung Road, Taoyuan 320, Taiwan, ROC
[c]Goldsun Development & Construction, Taipei 103, Taiwan, ROC

Received 27 March 2002; accepted 14 November 2003

Abstract

The aim of this study was to observe the behavior of the interfacial transition zone (ITZ) of high-performance concrete that was under curing in saturated lime water. From the Scanning Electron Microscope (SEM), it was found that the pores and hydration products at the ITZ, within 100 μm between the paste and aggregate, permuted each other during the early hydration stage, and then appeared as a large lump or strip. They gradually became irregular and small lumps for the further curing age. At the curing age of 56 days, the pores almost concentrated within an area of 0–15 μm from the aggregate edge. The hydration products were much denser with the increase in its distance from the aggregate edge.

Keywords: Interfacial transition zone; Water-to-binder ratio; Hydration products; Superplasticizers

1. Introduction

From their test, Hsu and Slate [1] observed that the bonding strength of interface was about 33% to 67% of the tensile strength of its cement matrix. Moreover, Slate and Matheus [2] and Buyukozturk et al. [3] observed that not only did an inattentive microscopically loose transition zone form near the area of the interface, but, also, an interfacial "separation crack" was caused possibly due to the shrinkage of cement matrix. Zaitsev [4] analyzed the fracture behavior of the concrete and found that the destruction began from the separation crack, which occurred first afterwards, along the interface of the aggregate and paste, and then advanced to the cement matrix when it reached a critical angle. Due to the expansion of the separation crack, the stress–strain curve appeared as a nonlinear behavior, and it limited the tensile stress of the concrete.

Bentur [5] observed the falling coarse aggregate within the concrete by scanning electron microscope (SEM). The coarse aggregate surface has an interfacial transition zone (ITZ) of about 100-μm depth. This ITZ includes two layers: One is a duplex film at the surface of the coarse aggregate, about 1 μm deep. Its components are CH crystals and C–S–H gels, as shown in Fig. 3. The other layer is the porous transition zone, about 20–100 μm deep, which contains more CH crystals, some C–S–H gels and little ettringite. Therefore, Bentur [5] concluded that the interface ought to include two weak faces, that is, a coarse aggregate surface (aggregate contact layer) and the porous transition zone (or called matrix contact layer). Both layers are collectively named as ITZ. These weak faces will influence the durability of concrete. With the progress of hydration, the discontinued pores of cement particles will be gradually filled with hydration products. Due to experimental difficulties, the information about the filled effect on transition zone is scarce.

Reference data about the properties of ITZ is little. According to Kumar Mehta's [6], Lea's [7] and Maso's [8] research, the structural characteristics of the transition zone can be obtained by the sequence of its development from the time concrete is placed. These characteristics are described as follows:

1. In freshly compacted concrete, water films form around the large aggregate particles. This would

* Corresponding author. Department of Civil Engineering, National Chiao Tung University, 10F-2, Number 10, Lane 157, Cihhuei, 3rd Street, 1001 Ta Hsueh Road, Hsinchu 300, Taoyuan County, Taiwan 320, Taiwan, ROC. Tel.: +886-3-4515811x612; fax: +886-3-4517602.
E-mail address: liawky@cc.vit.deu.tw (K.-Y. Liao).

0008-8846/$ – see front matter © 2004 Elsevier Ltd. All rights reserved.
doi:10.1016/j.cemconres.2003.11.019

Table 1
Character of cement, fly ash and aggregate used

Chemical composition (%)									
	SiO_2	Al_2O_3	Fe_2O_3	CaO	MgO	SO_3	Bl[a](cm^2/g)	Specific gravity	Ignition loss
Cement	20.49	6.57	3.27	62.40	1.91	2.20	3013	3.14	1.57
Fly ash	46.40	25.60	4.81	6.43	1.23	0.51	3920	2.20	10.65

	Density (g/cm^3)	Fineness modulus
Fine aggregate (sand)	2.63	2.83
Coarse aggregate	2.65	7.43

Superplasticizer Type	Solid content	Viscosity	Specific gravity	Water reduction rate
G	46.3%	2.5	2.5	23%

[a] Blaine specific surface area.

Table 2
Mixing proportion of concrete

W/B	Weight (kg/m^3)						Flash (cm)		45 min (cm)	
	Cement	Fly ash	Sand	Coarse aggregate	Water	SP	Slump	Slump flow	Slump	Slump flow
0.35	240	300	654	867	181	8	24	58	22	57
0.45	240	180	736	960	181	8	23	53	23	53
0.54	200	150	850	913	181	8	22	51	21	43
0.65	200	120	871	942	200	8	23	48	20	45

account for a higher water-to-cement ratio (W/C), closer to the larger aggregate than away from it (i.e., in the bulk mortar).

2. As in the bulk paste, calcium, sulfate, hydroxyl and aluminate irons are produced by the dissolution of calcium sulfate and calcium aluminate compounds, and are then combined to form ettringite and calcium hydroxide (CH). Owing to the higher water-to-cement ratio, these crystalline products in the vicinity of the coarse aggregate consist of relatively larger crystals. And, therefore, they form a more porous framework than in the bulk cement paste or mortar matrix.
3. With the progress of hydration, poor crystalline C–S–H and a second generation of smaller crystals of ettringite and CH start filling the empty space that exists between the framework created by the large ettringite and CH crystals. This helps improve the density and, hence, the strength of the transition zone.

When MIP is used to analyze the size of porous diameter, the distribution of the pores and the porosity, it can only be employed to observe the whole piece of the sample but not to explain a particular structure of the transition zone. Therefore, this research intended to inspect the structure in the range of 100 μm from the aggregate edge by using SEM, with magnification of ×2000. Continuous photographs were obtained by the photo-overlapping techniques, with the aid of a computer. Based on the contrast of different colors, we can identify and draw its porous positions to analyze the porous distribution of the transition zone. Utilizing the techniques of aeronautic and satellite survey system, and letting two neighbor SEM photographs overlap 60%, it is possible to make continuous photographs, with the aid of a computer. It gave an image with "depth", and thus allowed us to calculate the relative altitude of the crystals in the transi-

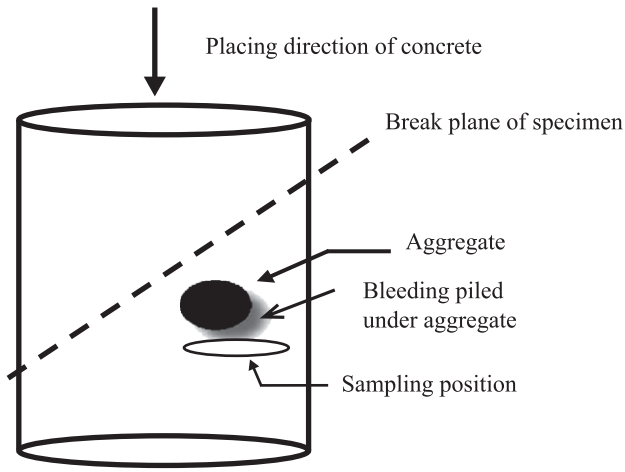

Fig. 1. The position of sampling.

Fig. 2. Ultrasonics.

tion zone, which revealed the variation of dense degree in this zone.

2. Test program

2.1. Materials

This research used Type I Portland cement, with a fineness of 301.3 m^2/kg (Blaine). The fly ash used is Type F fly ash produced by Taiwan Power. The superplasticizer used complied with ASTM C494 Type G and was considered as part of water. The solid content of the superplasticizer was 46.3%. For the chemical component and physical properties of cement, fly ash, superplasticizer and aggregate, see Table 1.

2.2. Mixture proportions

By referring to ACI 318-95 and Taiwan Concrete (TAICON) for the medium–low strength of concrete, the mixture proportions of this study were as follows: cement $\leqq 300$ kg/m^3, W/C $\geqq 0.42$. The slump test reached 22 ± 2 cm, and the flow-spread test was 50 ± 10 cm. After mixing for 45 min, the slump test was greater than or equal to 20 cm, and the flow-spread test was greater than or equal to 40 cm. The electrical resistivity of 56 days curing age was greater than 30 kΩ cm. The compressive strength of concrete was 28.5–35.7 MPa (280–350 kgf/cm^2), and the water-to-binder (W/B) ratios were 0.35, 0.45, 0.54 and 0.65, respectively. At mixture design, considering the economy and durability, the fixed quantity of water and superplasticizer was 181 and 8 kg/m^3, respectively. Then, let 1 kg cement provide the compressive strength of 0.14 MPa (1.4 kgf/cm^2), so that at W/B = 0.35, 0.45, the compressive strength is 35.7 MPa and the cement used is 240 kg/m^3, and at W/B = 0.54, 0.65, the compressive strength is 28.5 MPa and the cement used is 200 kg/m^3. The fly ash content was then adjusted to fit the request of slump and slump flow. The result of the mixture and slump are shown in Table 2.

Fig. 3. Resistivity measurements.

Fig. 4. Gilding instrument.

2.3. Curing condition

Considering that the hydration products of the concrete changed at different ages, in this test, the specimen was cured by limewater at room temperature (about 20–25 °C). Selected various ages of 1, 7, 14, 28 and 56 days were used to analyze the interfacial characteristics of paste and aggregate, and then to discuss the relationship between colossal and micro. One day curing age of this test was defined as the time spent for curing in saturate lime water after removing the concrete specimens from the mold; before that, the concrete was in the process of molding and put in air for 24 h. Actually, 1 day of curing age lasts 2 days.

2.4. Specimen making and sampling

According to the mixture of TAICON in making concrete specimen, after removing the concrete specimens from the

Fig. 5. Scanning electron microscope.

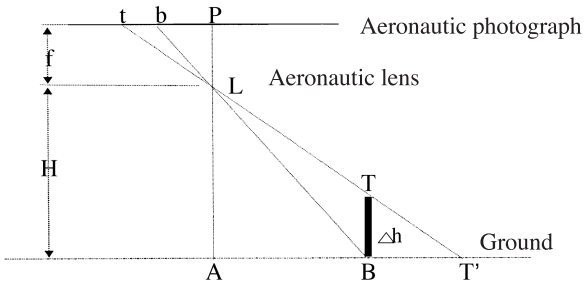

Fig. 6. Parallax variation of an aeronautic photograph.

mold, the specimen was put in saturated limewater. Until the plan curing age is reached, first, take the specimen and apply the pulse velocity and electrical resistivity tests, and then, the progress compressive test and sample a smaller sample to shoot using the SEM. This research discussed the characteristics of ITZ by aggregate surface. Hence, when sampling a smaller sample, the sample that includes aggregate and paste is put in methanol to stop hydration. The sampling position is shown in Fig. 1.

2.5. Supersonic test

Launch the supersonic wave through the concrete specimen and use the receiver to get the time. Then, set specimen length to calculate the supersonic speed for the test with both sides of the specimen daubed with lubricator. Use Ultrasonics (see Fig. 2) to measure the supersonic speed.

2.6. Electrical resistivity measuring

The concrete specimen was a nonhomogeneous material and utilizes inner different electric resistance caused by electric chemistry reaction to discuss its durability. To measure its electric resistance value, which can be obtained by four place of symmetry and average value, use resistivity measurement (see Fig. 3).

2.7. Calcium hydroxide content test

The thermogravimetric analysis instrument and differential thermogravimetric analysis instrument, acquired from TA Instruments, were deployed to determine the degree of hydration and the content of CH of the concrete samples, using the ignition method. The CH content of concrete was based on Eq. (1):

$$W_{CH} = 4.11(W_{440} - W_{580}) + 1.68(W_{580} - W_{1007}) / W_{1007} \times 100\% \quad (1)$$

where W_{CH} is the weight ratio of $Ca(OH)_2$ in the cement paste. W_{440}, W_{580} and W_{1007} are the weights of the specimens at 440, 580 and 1007 °C, respectively. The mass ratio of 1 mol $Ca(OH)_2$ to 1 mol H_2O is 4.11. The mass ratio of 1 mol $Ca(OH)_2$ to 1 mol CO_2 is 1.68.

2.8. SEM observation

Put the terminated hydration sample in the oven to dry for 24 h. From the dry sample, take a smaller sample (must both include aggregate and paste). After gilding, progress SEM observation, using the requisite equipment shown in Figs. 4 and 5. Under the SEM monitor, we must find out the interface of the aggregate and paste, and then take 10 sheets of continual SEM pictures from the aggregate edge toward the paste. Since the used magnification was ×2000, so that each photo has a 25-μm width, its right and left sides were retained with 7.5-μm overlap by each SEM picture; hence, the range of the combined 10-sheet continual SEM picture was 100 μm.

2.9. Three-dimensional inspection from SEM

To progress the three-dimensional inspection of SEM, quote the navigate photos to SEM. Fig. 6 explains the

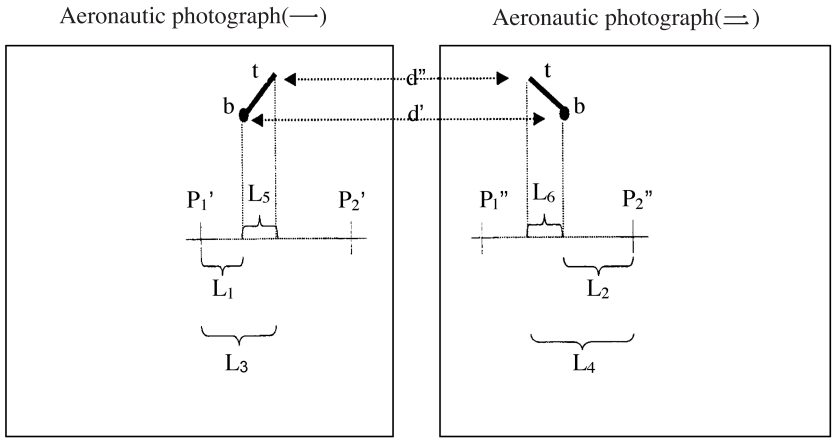

Fig. 7. The relationship of parallax by body TB at difference photograph.

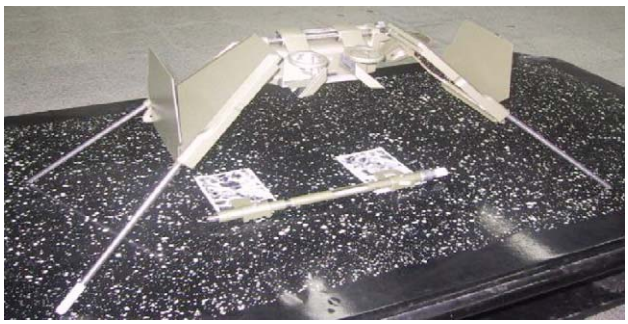

Fig. 8. The stereoscope and parallax ruler.

parallax variation of the navigate photos with an object on the ground—its top was T and the bottom was B. In navigate photos, the Position T changes to t and Position B changes to b due to the different distances from t or b to a main point P, which resulted from the difference in parallax values of the top and bottom points by same object. This phenomenon is called radioactive displacement. In the parallax relationship of two navigate photos shown in Fig. 7, the parallax of top point t was L3 + L4, and the parallax of bottom point b was L1 + L2, (L3 + L4) − (L1 + L2) =L5 + L6; this value was called ΔP. In making three-dimensional SEM photos, put two continual SEM pictures under a stereoscope (shown in Fig. 8), where the part which overlaps appears as three-dimensional, and mark numbers into the two continual SEM pictures. Use a parallax ruler to measure L1, L2, L3, L4 and the altitude, Ha, from the table to the stereoscope, the main point distance D (distance of marked number), and calculate ΔP, Pa. Utilizing Eq. (2), we can compute for Δh:

$$\Delta h = \{\Delta P/(\mathrm{Pa} + \Delta P)\}Ha \quad (2)$$

Each curing age takes about 30–40 points, with distributions in the ranges of 25–50, 50–75, 75–100 μm average, defining that the relation altitude of Point 1 was 100 units and the computation of the relation altitude of another point was based on this rate. Then, from different relation altitudes, it is possible to distinguish the density of hydration products within the transition zone. To let the situation of SEM inspection simulate in the same condition of aeronautic survey, when taking a SEM photograph, keep the camera lens moving horizontally.

3. Test results and discussion

3.1. Development of hydration products within transition zone for different ages

This SEM inspection covered mainly the range of 100 μm from the aggregate edge and uses a magnification of × 2000. Fig. 9 shows typical SEM microstructures produced by RGB color model. Although we cannot obtain the SEM inspection for different ages from the same sample, through the combination and comparison of several hundred photos, we can discover some inkling of the transition zone. The results for various ages from SEM are explained as follows:

Age of 1 day:

- At the edge of the aggregate, there are much unhydrated cement particles and products of initial hydration, which ranges from about 10 to 25 μm.
- From the SEM inspection, we can find a few C–S–H gels, but the hydration products of C–S–H increases quickly with the increase in curing age. The hydration products of C–S–H appeared as a needle-like shape, and the other hydration products, such as ettringite (AFt), monosulfate (AFm) and CH also exist as shown in Fig. 10. Moreover, we can find fly ash particles, obviously, as the fly ash are inactive at this age.

Age of 7 days:

- Monosulfate (AFm) increased suddenly, and was distributed in the range around 100 μm from the aggregate surface average. In other words, the unhydrated cement particles and products at the age of 1 day were transformed into monosulfate at the age of 7 days. Within the range of 10–25 μm, its crystal structure was much loose, whereas it became denser for the area beyond the range of 10–25 μm.
- The needle-shaped C–S–H increased and gradually formed the gel, with needles growing into the pore space just like mesh. At this age, the fly ash particles still did not react, but among the hydration products, pores existed.

Age of 14 days:

- We can find the C–S–H gel of mesh type. The C–S–H filled the mesh pores and, thus, the mesh structure was gradually formed as a plan structure. But the surface of the fly ash particles broke and dropped off gradually, and needle-shaped C–S–H was growing. This phenomenon explained that the partial surface of fly ash particles had started the pozzolanic reaction.
- The hydration products of ettringite (AFt) and monosulfate (AFm), as abundantly found by age of 7 days, can still be seen in this age, only that its amount was a little.

Age of 28 days:

- At the edge of the aggregate, there were still much hydration products caused by the pozzolanic reaction. Due to the mutual stack of these hydration products, it contained plenty of pores ranging from 20 to 50 μm. Beyond this range, we found that the previous pores were now filled with the hydration products of pozzolanic reaction, making the previous mesh structure turn into plan structure. This phenomenon was more obvious as

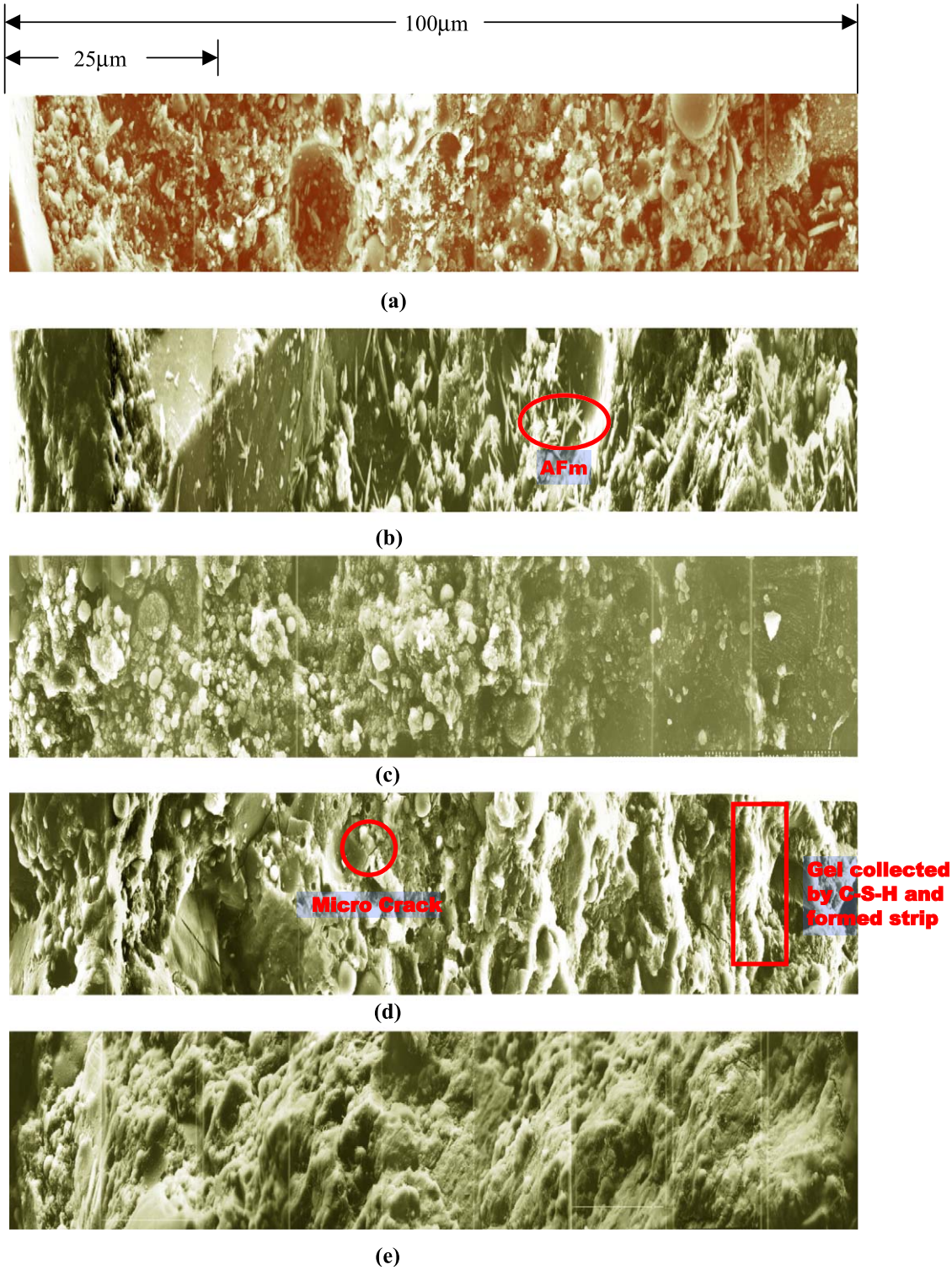

Fig. 9. Typical SEM Microstructures of transition zone of concrete curing with saturated lime water. (a) Typical SEM microstructures of the transition zone for 1 day (W/B = 0.35); (b) Typical SEM microstructures of the transition zone for 7 days (W/B = 0.45); (c) Typical SEM microstructures of the transition zone for 14 days (W/B = 0.54); (d) Typical SEM microstructures of the transition zone for 28 days (W/B = 0.54); (e) Typical SEM microstructures of the transition zone for 56 days (W/B = 0.54).

curing age increased. Moreover, from SEM microstructures, we found that the porosity decreased as the distance from the aggregate edge increased.

- From the observation, the fly ash particles kept on breaking and dropping off, and needle-shaped C–S–H was growing in it; but there were still some fly ash

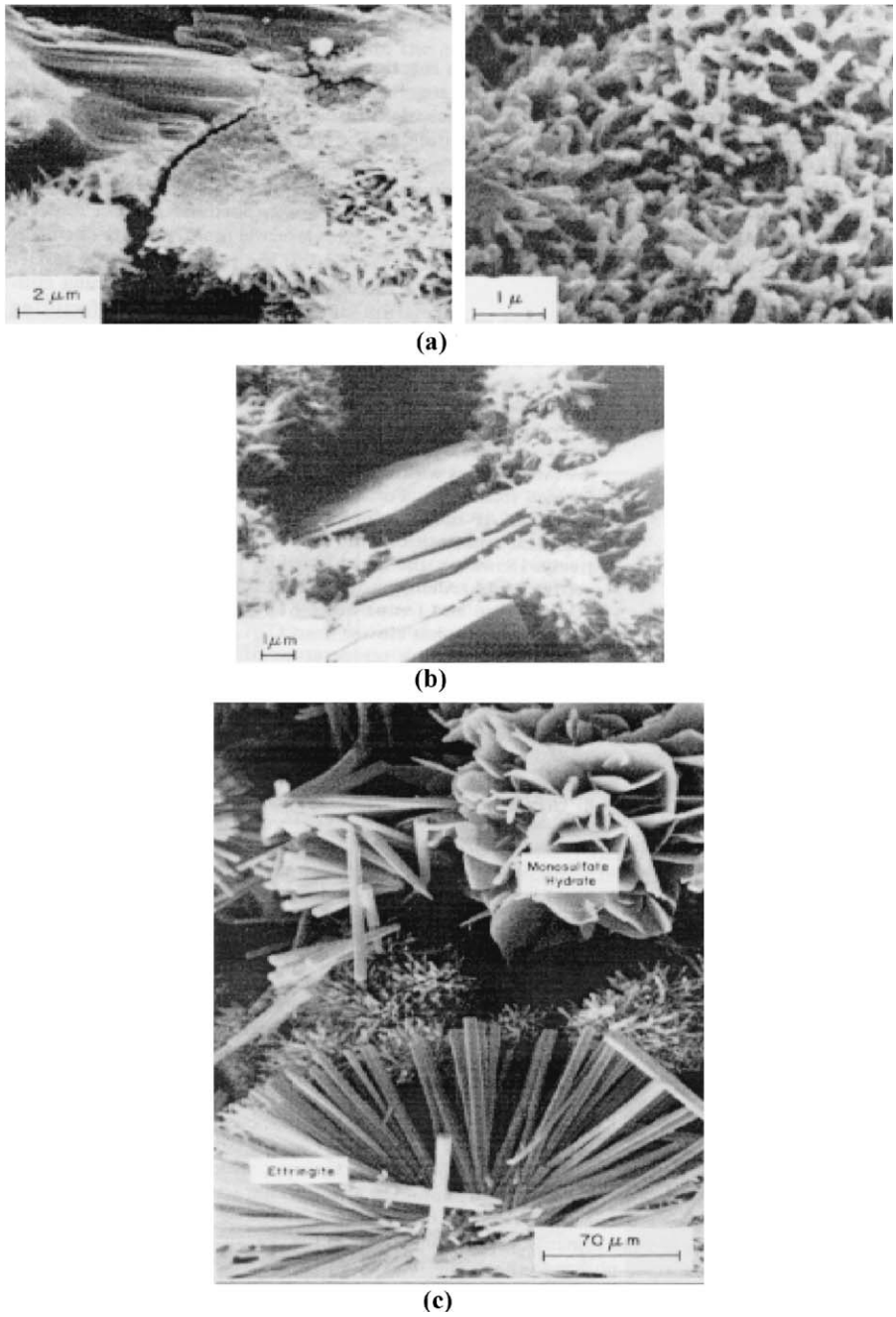

Fig. 10. Typical SEM Microstructures of (a) C–S–H, (b) CH and (c) Ettringite(Aft) and Monosulfate(Afm).

particles, which remained unreacted. The amount of CH was fewer than that in previous age, and this phenomenon explained that the CH was digested by the pozzolanic reaction.

Age of 56 days:

- At this time, the crystal structure was much denser, as can be seen in Fig. 9e. The pore size was less than that in the previous age. The C–S–H gel of mesh type was found, and plan structure was continuously formed. C–S–H gel of either mesh-type or spherical needle gel could be observed.
- It was observed that the particle size of fly ash decreases as the age increases because the fly ash structure was like a glass sphere. When its surface begins to react and drop off, its inner surface can react continuously and repeatedly, until all the fly ash completely reacted and fully filled the pore space.
- Around the aggregate edge, there still exist porous and loose hydration products, which ranges about 15–30 μm. Beyond this range was denser and intensive. Even

though the structure of the aggregate edge was loose, compared with the structure of the previous age, its interface structure is denser and firmer.

3.2. Development of porous structure in transition zone for different ages

Figs. 11 and 12 show the pore distribution diagrams of the transition zone, which were established for the range of 100 μm from the aggregate edge with SEM, using a magnification of ×2000 and the overlapping technique, to develop a continuous photograph. The difference color technique is employed to draw the pore's position, with the black portion being porous. Of course, owing to possible artificial mistakes, the selected place might not be a true structure pore, and the photograph used for analysis might not be a same sample. Therefore, the test data were used only for qualitative analysis. However, this research used an applicable drawing software to divide the pore positions and calculate its porosity. Therefore, using this method to

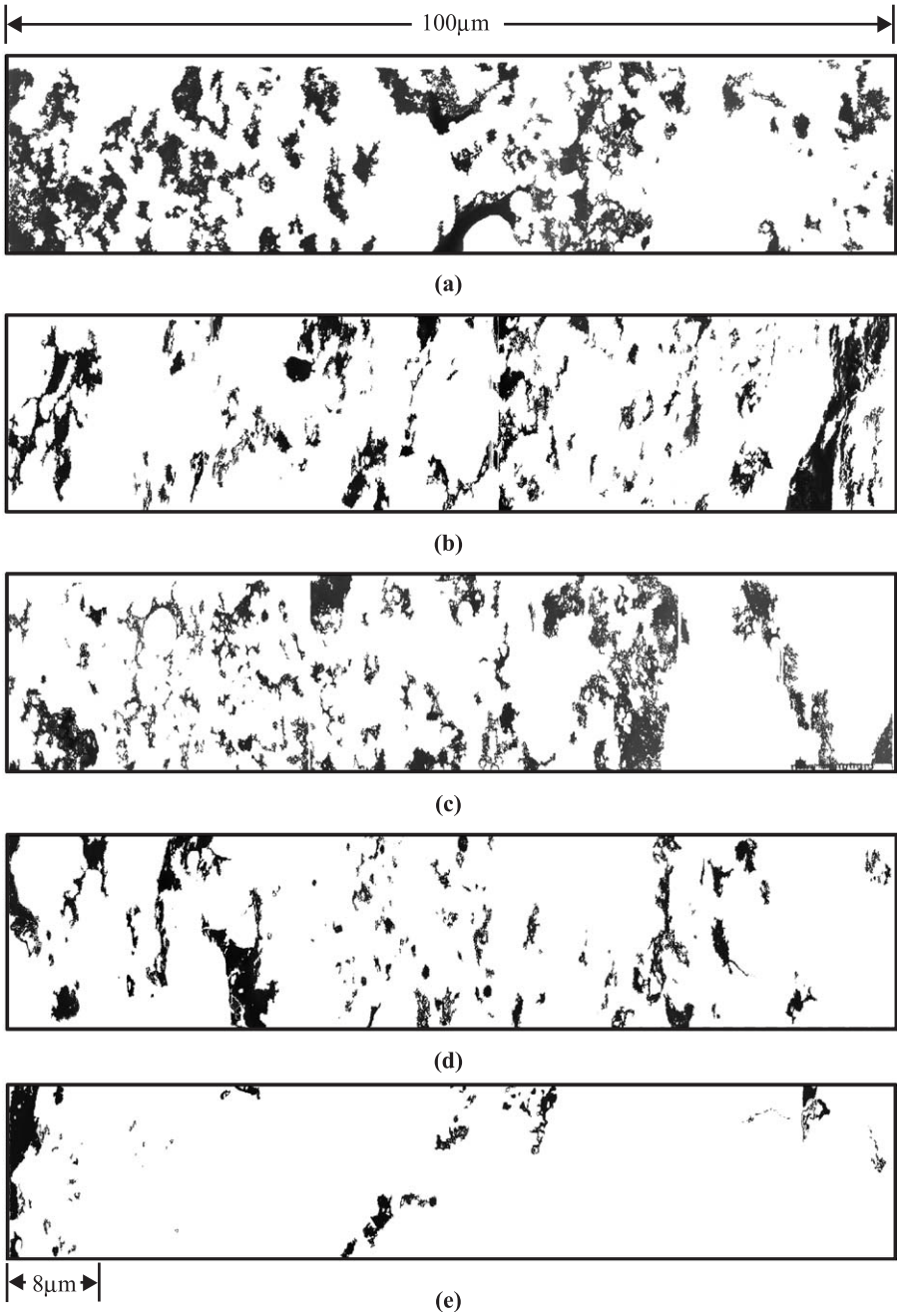

Fig. 11. The pore distribution of the transition zone of concrete curing with saturated lime water (W/B = 0.54) at (a) 1 day (porosity = 20.14%), (b) 7 days (porosity = 16.55%), (c) 14 days (porosity = 15.13%), (d) 28 days (porosity = 9.93%) and (e) 56 days (porosity = 3.51%).

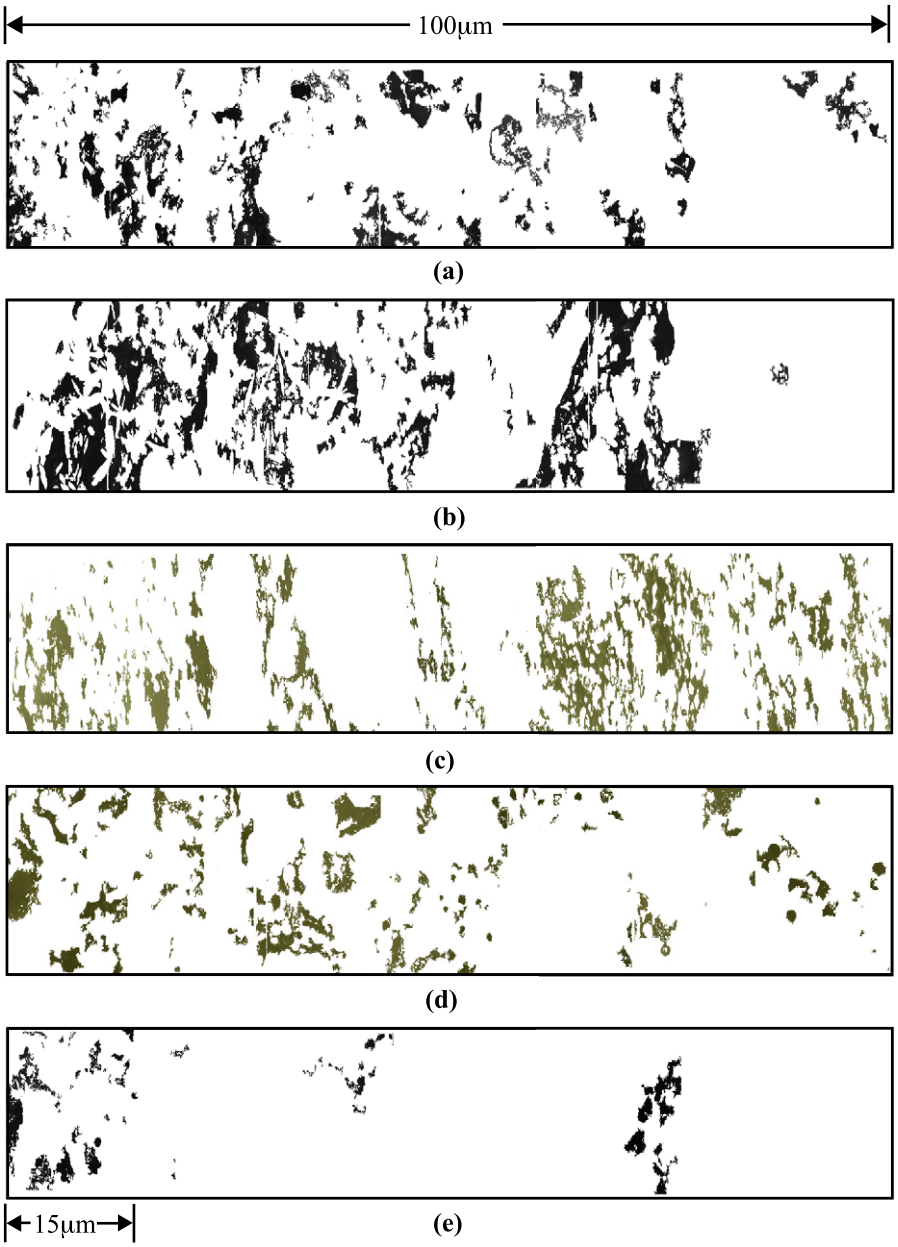

Fig. 12. The pore distribution of transition zone of concrete curing with saturated lime water (W/B = 0.65) at (a) 1 day (porosity = 20.44%), (b) 7 days (porosity = 19.01%), (c) 14 days (porosity = 16.56%), (d) 28 day (porosity = 10.60%) and (e) 56 days (porosity = 3.80%).

analyze the porosity structure of the transition zone was still a viable way.

From the SEM observation, at the age of 1 day, the pore distribution formed a large lump or strip, and the pores and hydration products were mutually permuted with each other. At the age of 7 days, previous phenomenon was more obvious, but the porous large lump or strip began to be divided into discontinuous ones. At the age of 14 days, the porous structure of large lump or strip formed a discontinuous strip, which was caused by the hydration products filling the pores. After 28 days, the distant place, which was originally porous, was now filled with the hydration products, and the pore structure was no more a strip type as in the early age, as shown in Figs. 11d and 12d. At the age of 56 days, pores concentrated in the aggregate edge, ranging from 0 to 15μm, as shown in Figs. 11e and 12e. Beyond this range, only few pores were distributed in a few small lumps. We defined the porous range of 56 days as the average thickness of the transition zone for HPC. From this research result, the average thickness of the transition zone for W/B = 0.54 and 0.65 was 0–15 μm, which was less than the 0–25 μm studied by Uchikawa et al. [9] for general Portland concrete, at W/C = 0.5 and age of 28–56 days. From the further calculation, it was found that porosity decreased with the increase in curing age. After the age of 14 days, the pores were

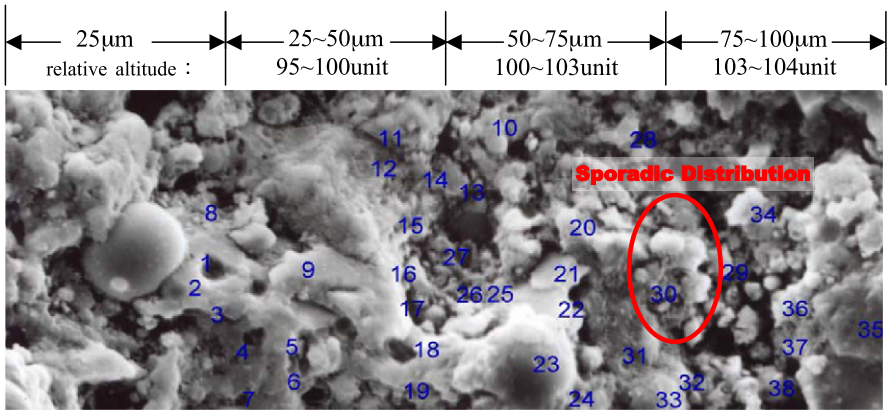

Fig. 13. The relative altitude of transition zone of concrete for 1 day curing with saturated lime water (W/B = 0.54). Relative altitude (the altitude of Point 1 is 100 units)—pt. 1: 100.000, pt. 2: 101.129, pt. 3: 98.342, pt. 4: 98.307, pt. 5: 99.177 pt. 6: 100.260, pt. 7: 100.000, pt. 8: 94.925, pt. 9: 99.869, pt. 10: 95.884, pt. 11: 98.290, pt. 12: 94.376, pt. 13: 95.776, pt. 14: 96.989, pt. 15: 96.863, pt. 16: 98.177, pt. 17: 99.724, pt. 18: 97.272, pt. 19: 98.625, pt. 20: 101.504, pt. 21: 100.544, pt. 22: 99.971, pt. 23: 103.558, pt. 24: 101.224, pt. 25: 99.566, pt. 26: 100.430, pt. 27: 100.658, pt. 28: 93.310, pt. 29: 101.916, pt. 30: 97.702, pt. 31: 97.606, pt. 32: 98.609, pt. 33: 104.934, pt. 34: 100.840, pt. 35: 102.591, pt. 36: 100.991, pt. 37: 100.749, pt. 38: 101.262.

filled due to the pozzolanic reaction, and the porosity was quickly reduced at the age of 28–56 days. This phenomenon proved that the pozzolanic reaction had promoted the durability of concrete.

3.3. Change of dense degree of hydration products in transition zone for different ages

Figs. 13–17 show the diagrams of dense degree of hydration products for W/B = 0.54, with ages of 1 to 56 days. At a distance of 25 μm from the edge of the aggregate, randomly take a point, named Point 1, and define its relation altitude as 100 unit, then randomly take some other points (about 30–40 points) at the range of 25–50, 50–75, 75–100 μm, and based on this rate, compute the relation altitude of another point. Because Point 1 was selected by random, if the Point 1 selected is the highest in all altitudes, the altitude of any other point will be less than that of Point 1 and vice versa. Therefore, it is not possible to compare the dense degree of hydration products with different curing ages; it is only possible to compare the dense degree of hydration products in the 100-μm range for the same curing age. According to the research by Kumar Mehta [6], Lea [7] and Maso [8] on freshly compacted concrete, water films form around the large aggregate particles, which would account for a higher water/cement ratio, closer to the larger aggregate than away from it, and more pores are formed. With the progress of hydration, hydration products start filling the empty space and make the hydration products denser than those away from the aggregate. This research utilized the survey techniques of aeronautic and satellite system, using the formula of Δh (Eq. 2 shown in Section 2.9) to estimate its relation altitude and observe the variation of

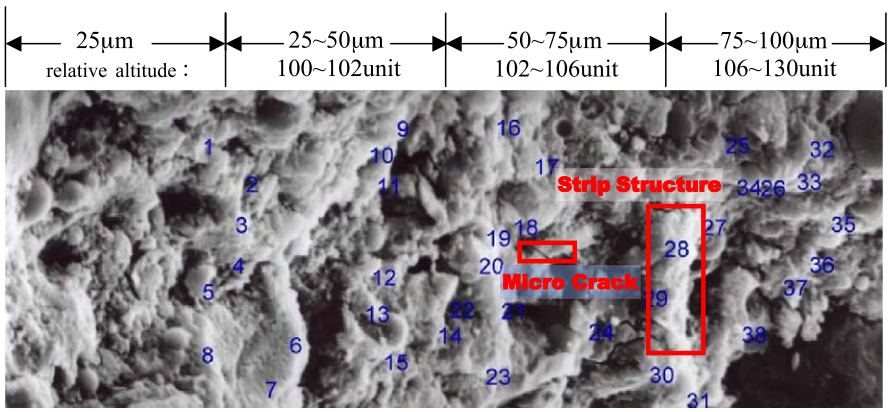

Fig. 14. The relative altitude of transition zone of concrete for 7 days curing with saturated lime water (W/B = 0.54). Relative altitude (the altitude of Point 1 is 100 units)—pt. 1: 100.000, pt. 2: 100.369, pt. 3: 100.436, pt. 4: 100.669, pt. 5: 99.732, pt. 6: 101.525, pt. 7: 102.077, pt. 8: 100.536, pt. 9: 99.631, pt. 10: 100.621, pt. 11: 100.235, pt. 12: 99.382, pt. 13: 101.525, pt. 14: 103.552, pt. 15: 100.447, pt. 16: 101.281, pt. 17: 103.371, pt. 18: 102.282, pt. 19: 103.371, pt. 20: 103.872, pt. 21: 103.586, pt. 22: 103.552, pt. 23: 106.236, pt. 24: 115.770, pt. 25: 118.491, pt. 26: 125.563, pt. 27: 119.922, pt. 28: 112.652, pt. 29: 112.112, pt. 30: 111.912, pt. 31: 118.127, pt. 32: 124.164, pt. 33: 124.292, pt. 34: 125.563, pt. 35: 127.901, pt. 36: 129.043, pt. 37: 127.025, pt. 38: 130.792.

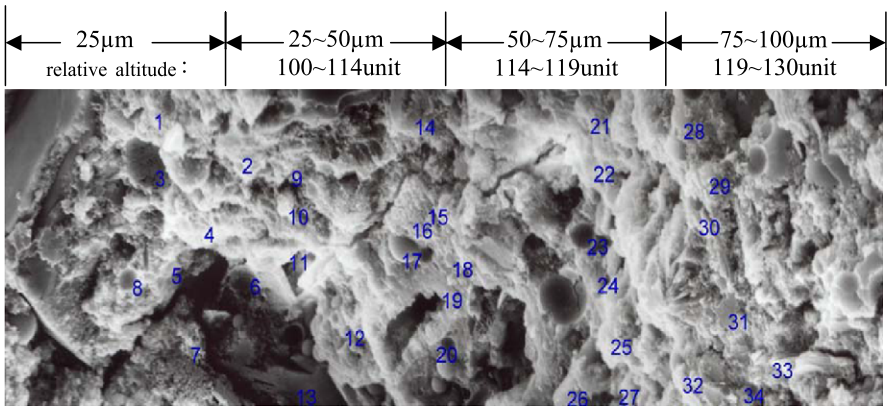

Fig. 15. The relative altitude of transition zone of concrete for 14 days curing with saturated lime water (W/B = 0.54). Relative altitude (the altitude of Point 1 is 100 units)—pt. 1: 100.000, pt. 2: 105.043, pt. 3: 101.322, pt. 4: 101.322, pt. 5: 100.096, pt. 6: 105.515, pt. 7: 101.785, pt. 8: 100.000, pt. 9: 106.109, pt. 10: 106.386, pt. 11: 107.749, pt. 12: 114.483, pt. 13: 112.068, pt. 14: 113.274, pt. 15: 116.192, pt. 16: 114.662, pt. 17: 115.608, pt. 18: 119.298, pt. 19: 117.399, pt. 20: 116.827, pt. 21: 113.672, pt. 22: 114.348, pt. 23: 110.048, pt. 24: 119.973, pt. 25: 125.394, pt. 26: 125.448, pt. 27: 127.628, pt. 28: 126.831, pt. 29: 126.088, pt. 30: 125.103, pt. 31: 126.432, pt. 32: 124.398, pt. 33: 130.311, pt. 34: 127.114.

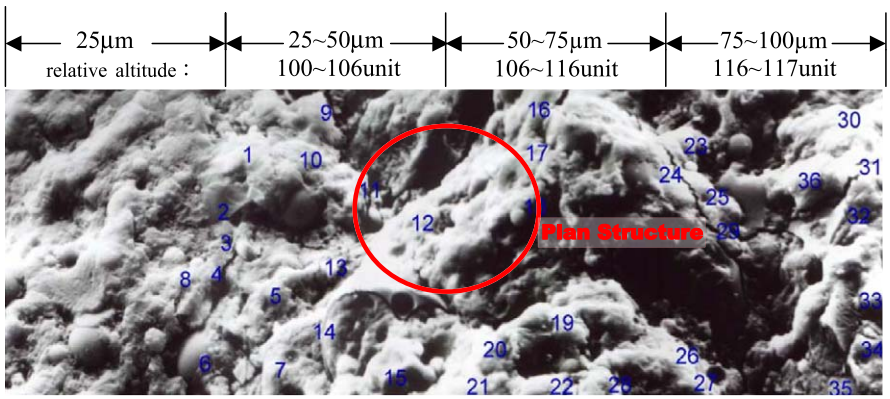

Fig. 16. The relative altitude of transition zone of concrete for 28 days curing with saturated lime water (W/B = 0.54). Relative altitude (the altitude of Point 1 is 100 units)—pt. 1: 100.000, pt. 2: 100.419, pt. 3: 100.252, pt. 4: 100.586, pt. 5: 102.985, pt. 6: 101.166, pt. 7: 104.277, pt. 8: 101.166, pt. 9: 101.573, pt. 10: 102.841, pt. 11: 103.842, pt. 12: 106.735, pt. 13: 103.890, pt. 14: 103.272, pt. 15: 105.744, pt. 16: 97.672, pt. 17: 102.498, pt. 18: 105.862, pt. 19: 119.595, pt. 20: 114.615, pt. 21: 115.475, pt. 22: 111.065, pt. 23: 111.222, pt. 24: 115.005, pt. 25: 116.798, pt. 26: 115.645, pt. 27: 116.327, pt. 28: 113.647, pt. 29: 116.641, pt. 30: 117.492, pt. 31: 117.227, pt. 32: 114.013, pt. 33: 116.748, pt. 34: 114.681, pt. 35: 113.563, pt. 36: 115.122.

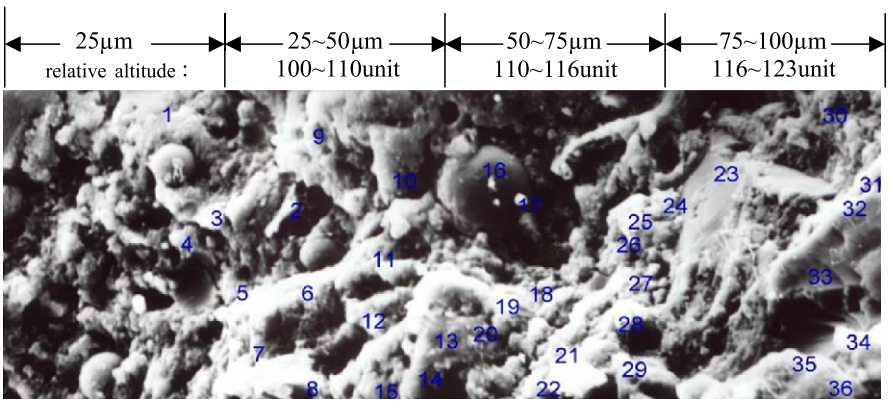

Fig. 17. The relative altitude of transition zone of concrete for 56 days curing with saturated lime water (W/B = 0.54).Relative altitude (the altitude of Point 1 is 100 units)—pt. 1: 100.000, pt. 2: 106.568, pt. 3: 103.353, pt. 4: 103.396, pt. 5: 104.757, pt. 6: 106.568, pt. 7: 106.850, pt. 8: 110.030, pt. 9: 105.343, pt. 10: 106.118, pt. 11: 107.633, pt. 12: 109.408, pt. 13: 112.015, pt. 14: 110.872, pt. 15: 109.533, pt. 16: 108.795, pt. 17: 110.578, pt. 18: 112.637, pt. 19: 111.554, pt. 20: 120.015, pt. 21: 115.257, pt. 22: 114.063, pt. 23: 120.912, pt. 24: 114.879, pt. 25: 113.727, pt. 26: 114.783, pt. 27: 115.445, pt. 28: 115.210, pt. 29: 116.517, pt. 30: 120.461, pt. 31: 123.894, pt. 32: 122.377, pt. 33: 120.642, pt. 34: 123.119, pt. 35: 121.136, pt. 36: 121.583.

dense degree. At the same time, defining a larger relation altitude, the hydration products are denser too. From Figs. 13–17, we can see the change of hydration products clearly: At the age of 1 day, the C–S–H gel appeared as a sporadic distribution in the range of 100 μm. From 7 to 14 days, the distribution from sporadic turned to strip; this phenomenon explained that the space of the sporadic distribution of the C–S–H gel was filled with hydration products and formed a strip distribution at 28 and 56 days. Due to being more filled again, let the C–S–H gel of strip distribution be collected to a large slice type called plan structure. Fig. 14 explains the relationship of relation altitude and dense degree of hydration products. From Fig. 14, we can find that in the ranges of 25–50, 50–75, 75–100 μm, the C–S–H gel's relative altitudes were 100–102, 102–106, 106–130 unit, namely, the relative altitudes were much higher with the increase in distance from aggregate edge. This phenomenon also proved that the hydration products were denser than those away from the aggregate, and found that the dense degree of hydration products was increased by distance increase from the aggregate edge at any curing age.

3.4. The relationship between colossal behavior and porous structure of the transition zone

Fig. 18a shows the development of the compressive strength of different mixture curings in saturated lime water for different ages. For any mixture, before 14 days, the development of compressive strength was controlled by W/C and cement quantity. Although the cement quantity used for W/B = 0.54 and W/B = 0.65 was the same, 200 kg/m^3, the mixing water used for W/B = 0.65 was 200 kg/m^3, higher than the 181 kg/m^3 used for W/B = 0.54. From Figs. 11 and 12, it is shown that the porosity of W/B = 0.65 was larger than that of W/B = 0.54, and thus, the compressive strength of W/B = 0.54 was higher than that of W/B = 0.65. They had the same tendency for strength development. From the SEM photograph at the of 14 days, as shown in Fig. 9c, it was found that the surface of fly ash particles broke and dropped off gradually to grow a needle-shaped C–S–H, which explained why the fly ash particles began to have a pozzolanic reaction. Thus, the interface condition between the aggregate and concrete paste improved, together with its promoted compressive strength. At the age of 28–56 days, the curve slope of the compressive strength quickly became large. This phenomenon denoted that W/C and cement quantity was the control factors of early compressive strength (before 14 days). W/B was a control factor of compressive strength during middle age (after 14 days), and this explains why ACI 318-95 defined W/B as a design factor of compressive strength and durability. At 56 days, the compressive strength of W/B = 0.54 adequately reached the design strength, but W/B = 0.65 nearly approached the compressive strength of the design; this explains that the fly ash quantity was an important factor of mixture design for high-performance concrete.

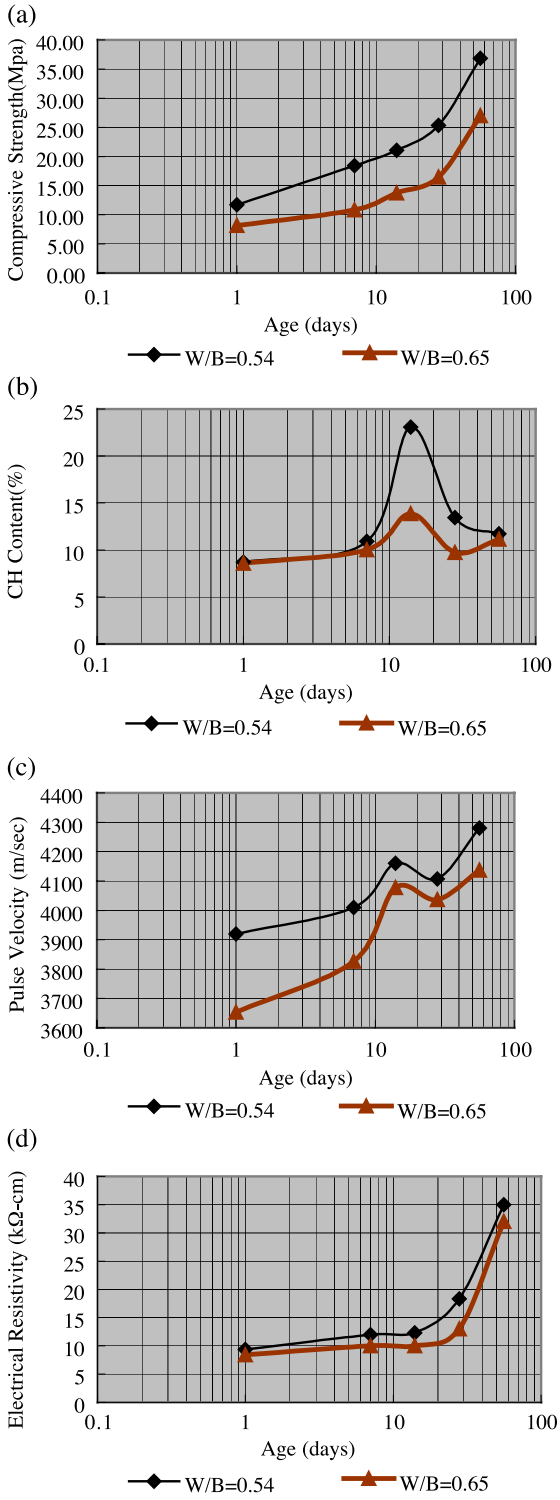

Fig. 18. The transmutation of (a) compressive strength, (b) CH content, (c) pulse velocity and (d) electrical resistance with different curing ages.

Fig. 18a and c shows the CH content and the development of pulse velocity for different mixture curing in saturated limewater for different ages. Before the age of

14 days, CH content and pulse velocity were growing with the increase in age, but in the age of 14–28 days, fly ash began to produce a pozzolanic reaction and consume calcium hydroxide, which resulted in the reduction of CH quantity and pulse velocity due to the fact that the rate of filling the pores was slower than that of the pores caused by microcrack as cement hydration.

For the electrical resistance of durability index (see Fig. 18d), before the age of 14 days, the compressive strength development was controlled by W/C, which shows that electrical resistance increased slowly (curve slope was gent). But at 14–56 days, electrical resistance increased quickly (curve slope was steeper), caused by C–S–H, which filled the pores again. This phenomenon explains that the fly ash was the best factor to promote the durability of concrete. They are all consistent with the principle that electrical resistance will be higher than 30 kΩ cm at the age of 56 days.

4. Conclusions

1. In the range (0–100 μm) of the transition zone, the hydration products change with the increase in curing age. At the age of 1 day, much unhydrated cement particles and a few of products of initial hydration, such as C–S–H and CH, existed in the area about 10–25 μm from the edge of the aggregate, with C–S–H appearing as a needle shape. At the age of 7 days, monosulfate (AFm) increased quickly and was distributed in the range of an average of 100 μm, with increased needle-shaped C–S–H, and gradually formed the mesh shape. At the age of 14 days, the C–S–H gel of mesh type was obviously developed, while the surface of the fly ash particles was broken and dropped off gradually, and a needle-shaped C–S–H grew. This phenomenon reveals that the fly ash particles have partially produced a pozzolanic reaction. At the age of 28 days, more hydration products were caused by the pozzolanic reaction at the edge of the aggregates; thus, the previous pores were filled by the hydration products of the pozzolanic reaction, making the previous mesh structure turn to plan structure. At the age of 56 days, the C–S–H gel of plan type was obviously found.
2. In the range (0–100 μm) of the transition zone, the density of the hydration products increased as the curing age increased, and the density of hydration products increased as the distance from the aggregate edge increased at any curing age.
3. In the range (0–100 μm) of the transition zone, the pores changed as the curing age increased. At the age of 1 day, the area of the pores was at its highest, and the pores were distributed uniformly in the whole range in a large lump or strip. At the age of 7 days, there were also many pores in the whole range, but the pores of large lump or strip began to divide into discontinuous situations. At the age of 14 days, the C–S–H gel formed to become a mesh structure and, thus, the pores became a discontinuous strip. At the age of 28 days, the pozzolanic reaction products filled most of the pores and, thus, the pores and porosity were reduced quickly to the range of 25–100 μm. At the age of 56 days, all the pores concentrated in the aggregate edge.
4. From the porous structure diagram of transition zone, at the age of 56 days, it was found that, in the range of 0–15 μm away from the aggregate edge, there are still many pores, but in the range of 15–100 μm, more hydration products existed with only a little amount of pores resulting in a denser structure. Hence, it can be concluded that in the transition zone, the weakest place was at the range of 0–15 μm.

Acknowledgements

The authors would like to thank the National Science Council of the Republic of China for the financial support (Grant No.: NSC 89-2211-E-009-087).

References

[1] T.T.C. Hsu, F.O. Slate, Tensile bond between aggregate and cement paste or mortar, J. Am. Concr. Inst. Proc. 60 (2) (1963) 465–486.
[2] F.O. Slate, R.F. Matheus, Volume changes on setting and curing of cement paste and concrete from zero to seven days, J. Am. Concr. Inst. Proc. 64 (1967) 34–39.
[3] O. Buyukozturk, A.H. Nilson, F.O. Slate, Stress–strain response and fracture of a concrete model in biaxial loading, J. Am. Concr. Inst. Proc. 68 (1971) 590–599.
[4] Yu.V. Zaitsev, in: F.H. Wittmann (Ed.), Crack Propagation in a Composite Material, Fracture Mechanics of Concrete, 1983.
[5] A. Bentur, Microstructure interfacial effects and micromechanics of cementitious composites, Adv. Cementitious Mater., Ceram. Trans. 16 (1990) 523–549.
[6] P. Kumar Mehta, Concrete Structure, Properties and Materials, Prentice-Hall, Englewood Cliffs, NJ, 1986.
[7] F.M. Lea, The Chemistry of Cement and Concrete, Chemical Publishing, New York, 1971.
[8] F. Maso, Proceedings of the Seventh International Congress on the Chemistry of Cements, Editions Septima, Paris, 1980.
[9] H. Uchikawa, S. Hanehara, D. Sawaki, Estimation of the thickness of transition zone in hardened mortar and concrete, and investigation of the relationship between their thickness and strength development, concrete research and technology, Jpn. Concr. Inst. 4 (2) (1993) 1–8.